J|A|C|S ARTICLES

Published on Web 02/23/2010

Outer Wall Selectively Oxidized, Water-Soluble Double-Walled Carbon Nanotubes

Alexandra H. Brozena,[†] Jessica Moskowitz,[†] Beiyue Shao,[†] Shunliu Deng,[†,‡] Hongwei Liao,[†] Karen J. Gaskell,[†] and YuHuang Wang*[,†,§]

Department of Chemistry and Biochemistry, University of Maryland, College Park, Maryland 20742, Department of Chemistry, Xiamen University, Xiamen, Fujian, China, and Maryland NanoCenter, University of Maryland, College Park, Maryland 20742

Received December 16, 2009; E-mail: yhw@umd.edu

Abstract: The outer walls of double-walled carbon nanotubes (DWNTs) were selectively oxidized using a combination of oleum and nitric acid. Intercalation of oleum between bundled DWNTs enabled a homogeneous reaction by equally exposing all outer wall surfaces to the oxidants. At optimized reaction conditions, this double-wall chemistry enabled high water solubility through carboxylic acid functional groups introduced to the outer wall, while leaving the inner tube intact, as shown by Raman scattering and high resolution TEM. These outer wall selectively oxidized DWNTs retained electrical conductivity up to 65% better than thin films of similarly functionalized single-walled carbon nanotubes, which can be attributed to enhanced electrical percolation via the nonoxidized inner tubes.

Introduction

Single-walled carbon nanotubes (SWNTs) combine remarkable electrical, mechanical, thermal, and optical properties,[1,2] yet the lack of solubility in conventional solvents is a serious drawback to their applications in a number of important areas, including composite materials,[3,4] biomedicine,[5] and solar cells.[6,7] The insolubility is due to the inert graphitic nature and strong intertube van der Waals interactions.[8,9] Over the past decade, enormous efforts have been devoted to addressing this insolubility problem.[8,10−13] The most successful approaches to date have involved either covalent side-wall functionalization chemistry[12,13] or noncovalent processes that rely on the use of surfactants or polymers to form kinetically stable suspensions.[8,10,11] However, choosing between covalent and noncovalent approaches involves an unattractive trade-off. Noncovalent approaches typically suffer from large amounts of surfactant/polymer contamination, low yields, and limited scalability.[8,10,11] Covalent sidewall chemistries can overcome these problems and effectively render SWNTs soluble as thermodynamically stable solutions.[12,13] Unfortunately, covalent chemistry dramatically alters the atomic and electronic structures of SWNTs,[14] causing the loss of the electrical properties[15] and the degradation of their mechanical strength and chemical stability.

Here we report outer wall selectively oxidized double-walled carbon nanotubes (*oso*-DWNTs) as a promising materials strategy to address this insolubility problem. DWNTs are a class of carbon nanostructures composed of exactly two graphene sheets that are conceptually rolled in concentric tubes. A series of recent advances have shown that DWNTs exhibit a range of interesting electrical,[16] thermal,[17] and mechanical properties[18] that are sometimes superior to SWNTs. By adapting an acid oxidation chemistry previously used on SWNTs,[19,20] we have demonstrated outer wall selective oxidization of DWNTs to the

[†] Department of Chemistry and Biochemistry, University of Maryland.
[‡] Xiamen University.
[§] Maryland NanoCenter, University of Maryland.

(1) Saito, R.; Dresselhaus, G.; Dresselhaus, M. S. *Physical Properties of Carbon Nanotubes*; Imperial College Press: London, 1998.
(2) Baughman, R. H.; Zakhidov, A. A.; de Heer, W. A. *Science* **2002**, *297*, 787–92.
(3) Ajayan, P. M.; Tour, J. M. *Nature* **2007**, *447*, 1066–1068.
(4) Vigolo, B.; Coulon, C.; Maugey, M.; Zakri, C.; Poulin, P. *Science* **2005**, *309*, 920–923.
(5) Liu, Z.; Tabakman, S.; Welsher, K.; Dai, H. *Nano Res.* **2009**, *2*, 85–120.
(6) Rahman, G. M. A.; Guldi, D. M.; Cagnoli, R.; Mucci, A.; Schenetti, L.; Vaccari, L.; Prato, M. *J. Am. Chem. Soc.* **2005**, *127*, 10051–10057.
(7) Kongkanand, A.; Martinez Dominguez, R.; Kamat, P. V. *Nano Lett.* **2007**, *7*, 676–680.
(8) O'Connell, M. J.; Boul, P.; Ericson, L. M.; Huffman, C.; Wang, Y.; Haroz, E.; Kuper, C.; Tour, J.; Ausman, K. D.; Smalley, R. E. *Chem. Phys. Lett.* **2001**, *342*, 265–271.
(9) Sun, C.-H.; Yin, L.-C.; Li, F.; Lu, G.-Q.; Cheng, H.-M. *Chem. Phys. Lett.* **2005**, *403*, 343–346.
(10) O'Connell, M. J.; Bachilo, S. M.; Huffman, C. B.; Moore, V. C.; Strano, M. S.; Haroz, E. H.; Rialon, K. L.; Boul, P. J.; Noon, W. H.; Kittrell, C.; Ma, J.; Hauge, R. H.; Weisman, R. B.; Smalley, R. E. *Science* **2002**, *297*, 593–596.
(11) Zhao, Y.-L.; Stoddart, J. F. *Acc. Chem. Res.* **2009**, *42*, 1161–1171.
(12) Tasis, D.; Tagmatarchis, N.; Bianco, A.; Prato, M. *Chem. Rev.* **2006**, *106*, 1105–1136.
(13) Peng, X.; Wong, S. S. *Adv. Mater.* **2009**, *21*, 625–642.
(14) Park, H.; Zhao, J.; Lu, J. P. *Nano Lett.* **2006**, *6*, 916–919.
(15) Strano, M. S.; Dyke, C. A.; Usrey, M. L.; Barone, P. W.; Allen, M. J.; Shan, H.; Kittrell, C.; Hauge, R. H.; Tour, J. M.; Smalley, R. E. *Science* **2003**, *301*, 1519–1522.
(16) Liu, K.; Wang, W.; Xu, Z.; Bai, X.; Wang, E.; Yao, Y.; Zhang, J.; Liu, Z. *J. Am. Chem. Soc.* **2009**, *131*, 62–63.
(17) Kim, Y. A.; Muramatsu, H.; Hayashi, T.; Endo, M.; Terrones, M.; Dresselhaus, M. S. *Chem. Phys. Lett.* **2004**, *398*, 87–92.
(18) Peng, B.; Locascio, M.; Zapol, P.; Li, S.; Mielke, S. L.; Schatz, G. C.; Espinosa, H. D. *Nat. Nanotechnol.* **2008**, *3*, 626–631.
(19) Liu, J.; Rinzler, A. G.; Dai, H.; Hafner, J. H.; Bradley, R. K.; Boul, P. J.; Lu, A.; Iverson, T.; Shelimov, K.; Huffman, C. B.; Rodriguez-Macias, F.; Shon, Y.-S.; Lee, T. R.; Colbert, D. T.; Smalley, R. E. *Science* **1998**, *280*, 1253–1256.
(20) Chen, Z.; Kobashi, K.; Rauwald, U.; Booker, R.; Fan, H.; Hwang, W.-F.; Tour, J. M. *J. Am. Chem. Soc.* **2006**, *128*, 10568–10571.

10.1021/ja910626u

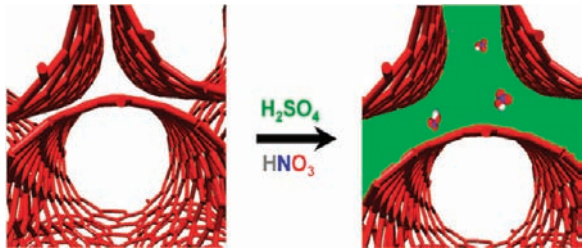

Figure 1. Schematic illustration of outer wall selective oxidation of DWNTs by H_2SO_4/HNO_3. H_2SO_4 intercalation opens the diffusion pathways for HNO_3 to access nanotubes embedded in a rope and react with the exposed outer walls selectively. For clarity, the inner tubes are omitted.

exclusion of the inner tubes. This "double-wall" chemistry produced water-soluble materials while preserving the electrical properties of the inner tube.

Specifically, DWNTs were dispersed in oleum (100% H_2SO_4 with excess SO_3) and then reacted with nitric acid to afford *oso*-DWNTs that are highly soluble in water. Over 70% of DWNTs became soluble in water with a yield better than 70% from the starting material. Unlike conventional organic covalent chemistry[12,13] or gas phase reactions,[13] the intercalation of oleum between bundled nanotubes[21,22] presumably opens the diffusion pathways for the HNO_3 to equally access all outer wall surfaces (Figure 1). We believe this intercalation diffusion mechanism allows the reaction to occur homogeneously at high concentrations. The diffusion mechanism may also include epoxidation[23,24] of the bundled DWNT ends with the potential for these groups to migrate across the surface. However, the calculated rate of epoxide migration by density functional theory is only once every 100 s at room temperature[24] and is therefore not considered to be the major contributor of DWNT oxidation in this experiment.

The functionalized DWNTs were systematically characterized with Raman spectroscopy, UV−visible spectroscopy, X-ray photoelectron spectroscopy (XPS), and high resolution TEM. These results reveal strong correlations between solubility and degree of functionalization with the relative reactant concentration and reaction time in addition to displaying outer wall selectivity at optimized reaction conditions. Outer wall selectivity was found essential in retaining the electrical conductivity of *oso*-DWNT thin films by efficient inner-tube pathways that are absent in functionalized SWNTs films. These results demonstrate a possible solution to the covalent-modification trade-off between water solubility and the desirable electrical properties associated with these structures.

Experimental Procedures and Methods

Outer Wall Selective Oxidation of Superacid Intercalated DWNTs. 50 mg of raw DWNTs (Unidym DW411UA) were added to 50 mL of oleum in a three-necked flask (reagent grade, 20% free SO_3 basis, Sigma Aldrich) (*Warning: oleum is very corrosive and should be treated with caution*). The spontaneously formed black, homogeneous solution was stirred for 24 h under argon protection to ensure complete intercalation by oleum, after which the dispersion was heated in a water bath to 65 °C. 70% HNO_3 (Certified ACS Plus, Fischer Scientific; 1−20 mL) was added drop by drop through an addition funnel to the solution (*Warning: nitric acid is extremely corrosive and should be treated with caution*). The solution was left to react for 2−24 h. The conditions investigated include a 2 h reaction time with added nitric acid volumes of 1, 5, 10, and 20 mL. Additional conditions include reacting 5 mL of nitric acid for 2, 12, and 24 h. This fixed 5 mL reactant volume was chosen to avoid immediate overoxidation of the sample, allowing the reaction to be studied over longer periods of time than if a 10 mL fixed volume were chosen. When the desired reaction time was reached, the solution was removed from the warm bath and left in air to cool for 10 min. The black slurry was slowly added into 250 mL of nanopure water (18.2 MΩ), with a glass stir rod to prevent splashing. The diluted DWNT solution was vacuum filtrated. The filtered DWNTs were then washed with 100 mL of diethyl ether and 50 mL of methanol. Finally, the DWNTs were washed with 1 L of nanopure water to ensure that the DWNTs were acid free. The solids were placed in a vacuum oven at 80 °C for 12 h to dry. These experimental procedures ensured that the samples were free of the chemical doping effects by acids.[25]

Relative Solubility of Oxidized DWNTs Prepared at Different Reaction Conditions. To determine which oxidative conditions (in terms of reactant concentration and reaction time) resulted in the most soluble sample, a hexane and water extraction procedure was developed to separate the water-soluble and insoluble DWNTs. 3.0 mg of each oxidized DWNT sample were sonicated using a Misonix S-4000 ultrasonicator (Farmingdale, NY) at ∼115 W in 18 mL of basic (pH ∼9) nanowater for 25 min. 7 mL of hexane (99.5%, Pharmco-AAPER) were then added to the water dispersion and shaken by hand in a sealed vial. After 25 min, the mixture was phase separated into two distinct layers with water-soluble DWNTs on the bottom aqueous layer. The concentration of the functionalized DWNTs that were water soluble was determined by the absorbance of the aqueous solution, which was measured using a Perkin-Elmer 1050 UV−vis−NIR spectrophotometer (Waltham, Massachusetts). The concentration was determined optically at $\lambda = 500$ nm from absorbance vs concentration working curves of raw DWNTs dispersed in nanopure water using 1 wt % sodium dodecyl sulfonate (SDS).

Determining Maximum Water Solubility of Oxidized DWNTs. To find the maximum water solubility, 16.6 mg of the oxidized DWNT sample were dispersed in 10 mL of NaOH aqueous solution (pH ∼10) and sonicated at ∼115 W for 1 h in a circulated cooling water bath. 1 mL of the dispersed solution was added to three centrifuge tubes each, which were then centrifuged at 2800 g for 60 min. After centrifugation, 0.10 mL of the top layer solution was taken from each vial and diluted 80 times. The UV−vis−NIR spectra were taken for each of the diluted solutions. This centrifugation and absorbance measurement procedure was repeated for the remaining 0.90 mL dispersions in each centrifuge tube under the same conditions for a total of 5 times, after which the UV−vis−NIR spectra reached a constant. At this state, the dispersion was expected to be at its most stable state where the maximum solubility of the functionalized DWNTs was calculated by the aforementioned optical method.

X-ray Photoelectron Spectroscopy. XPS data were collected on a Kratos Axis 165 (Manchester, U.K.) operating in hybrid mode using monochromatic Al Kα radiation (1486.6 eV) at 240 W. The samples were mounted on double sided carbon tape, and the pressure of the instrument remained below 1×10^{-8} Torr throughout the data collection. Survey spectra were collected at a pass energy of 160 eV, while high resolution spectra were collected at a pass energy of 20 eV. All peaks were calibrated to the sp^2 hybridized peak at 284.5 eV and, after the application of a Shirley

(21) Davis, V. A.; Ericson, L. M.; Parra-Vasquez, A. N. G.; Fan, H.; Wang, Y.; Prieto, V.; Longoria, J. A.; Ramesh, S.; Saini, R. K.; Kittrell, C.; Billups, W. E.; Adams, W. W.; Hauge, R. H.; Smalley, R. E.; Pasquali, M. *Macromolecules* **2004**, *37*, 154–160.
(22) Ericson, L. M.; Fan, H.; Peng, H.; et al. *Science* **2004**, *305*, 1447–1450.
(23) Paci, J. T.; Belytschko, T.; Schatz, G. C. *J. Phys. Chem. C* **2007**, *111*, 18099–18111.
(24) Li, J.-L.; Kudin, K. N.; McAllister, M. J.; Prud'homme, R. K.; Aksay, I. A.; Car, R. *Phys. Rev. Lett.* **2006**, *96*, 176101/1–176101/4.
(25) Kaempgen, M.; Lebert, M.; Haluska, M.; Nicoloso, N.; Roth, S. *Adv. Mater.* **2008**, *20*, 616–620.

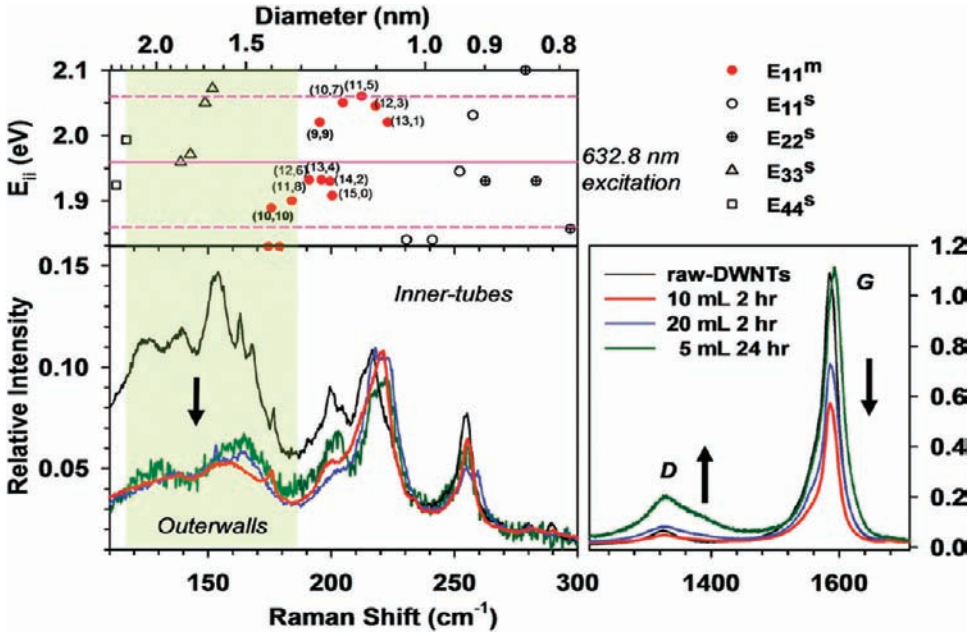

Figure 2. Raman spectral evidence of outer wall selectivity. The Raman spectra of the oxidized DWNTs under different reaction conditions (red line: 10 mL HNO_3 2 h; blue line: 20 mL 2 h; green line: 5 mL 24 h) were plotted in comparison with that of raw DWNTs (black line). The intensities were normalized to the peak centered around 215 cm^{-1}. The shaded area is dominated by outer walls. The metallic inner tubes (red circles) are indicated by the above Kataula plot, where the excitation window of the laser used ($\lambda = 632.8$ nm) is indicated by the two dotted lines.

background,[26] fit with peaks with a 70% Gaussian 30% Lorentzian product function. The graphitic peak was modified with an asymmetric form A(0.4,0.55,30)GL(30) determined through fitting of the pristine nanotube C 1s spectrum, using CasaXPS software.

Raman Spectroscopy. Raman scattering data were collected on a Horiba Jobin Yvon LabRAM HR800 Raman microscope (Edison, NJ) using 632.8, 514.5, and 488.0 nm excitation lines. The nonpartitioned samples of the DWNTs (including both water-soluble and insoluble fractions) were dispersed in ethanol by brief sonication to improve uniformity and deposited dropwise on a glass microscope slide using a Pasteur pipet and allowed to dry. Spectra for each sample were obtained by measuring the Raman scattering of three separate spots on each sample and averaged.

Transmission Electron Microscopy (TEM) and Scanning Electron Microscopy (SEM). TEM images of the 5 mL 24 h and 10 mL 2 h samples were obtained using a JEOL JEM-2100 LaB6 transmission electron microscope (Tokyo, Japan) at a 200 kV accelerating voltage. High resolution images were taken on a JEOL JEM 2100 FEG transmission electron microscope (Tokyo, Japan) at the same accelerating voltage. Nonpartitioned DWNT samples were washed with nanopure water to protonate surface carboxylic acid functional groups and then dispersed in ethanol. These solutions were then briefly sonicated and deposited on an SPI lacey carbon coated 300 mesh copper grid (West Chester, Pennsylvania) using a Pasteur pipet.

Length distributions of the raw, 5 mL 24 h and 10 mL 2 h samples were measured by SEM on a Hitachi SU-70 SEM (Tokyo, Japan) at a 3 kV accelerating voltage. The raw DWNT sample was first dispersed in 1,2-dichlorobenzene and spin-coated on a silicon wafer at 3000 rpm. The 5 mL 24 h and 10 mL 2 h samples were resuspended in ethanol, followed by deposition on a silicon wafer by spin-coating. The images were then analyzed using ImageJ software.

Carbon Nanotube Thin Film Conductivity Measurements. Functionalized DWNT samples and HiPco SWNT controls[27] (received as a gift from Rice University) were weighed and resuspended in ethanol by sonication to form a 0.20 mg/mL solution. The oxidized SWNT sample was functionalized at the same conditions as the 10 mL 2 h DWNT sample. The solution was filtrated through a 0.2 μm GTTP Isopore Membrane (Millipore) to form a thin film. The thin film was cut into 0.20−0.32 cm wide strips. Electrodes (5 nm Cr/50 nm Au) were deposited on the strip through a shadow mask using thermal evaporation (Metra Evaporator, Metra, Inc.) to form a 0.50 cm long conducting channel. Resistances were measured with a multimeter. The film thickness was estimated using the film area and density (1.3 g/cm^3).

Results and Discussion

Raman, XPS, and water solubility data clearly indicate the successful functionalization of the DWNT samples, but most interesting was the evidence of outer wall selectivity. Figure 2 shows the Raman spectra of the oxidized DWNTs under different reaction conditions. The most pronounced Raman signatures of a DWNT arise from scattering by the radial breathing modes (RBMs) in the range 100−350 cm^{-1} and C−C tangential modes around 1500−1600 cm^{-1}, which are collectively known as the G band.[28] Oxidation introduces sp^3 centers and other structural defects, which give rise to the so-called D band around 1350 cm^{-1}.[28] Importantly, due to relatively weak interwall interactions within a DWNT, each of the two constituent walls will give a different set of Raman peaks.[29] In particular, the inner tube and the outer wall have distinct RBMs because the low frequency Raman shifts are inversely proportional to the nanotube diameter.[28,30] We attributed the raw-DWNT peaks at approximately 150 cm^{-1} and 215 cm^{-1} to the RBMs of the outer walls and inner tubes, respectively. After

(26) Shirley, D. A. *Phys. Rev. B* **1972**, *5*, 4709–14.
(27) Bronikowski, M. J.; Willis, P. A.; Colbert, D. T.; Smith, K. A.; Smalley, R. E. *J. Vac. Sci. Technol., A* **2001**, *19*, 1800–1805.
(28) Dresselhaus, M. S.; Dresselhaus, G.; Jorio, A. *J. Phys. Chem. C* **2007**, *111*, 17887–17893.
(29) Endo, M.; Muramatsu, H.; Hayashi, T.; Kim, Y. A.; Terrones, M.; Dresselhaus, M. S. *Nature* **2005**, *433*, 476.
(30) Villalpando-Paez, F.; Son, H.; Nezich, D.; Hsieh, Y. P.; Kong, J.; Kim, Y. A.; Shimamoto, D.; Muramatsu, H.; Hayashi, T.; Endo, M.; Terrones, M.; Dresselhaus, M. S. *Nano Lett.* **2008**, *8*, 3879–3886.

oxidation, the peaks centered around 150 cm^{-1} were depressed. However these same samples retain the peaks centered around 215 cm^{-1} corresponding to the inner tubes of the DWNTs. The retention of the inner tubes' RBMs and the simultaneous disappearance of those of the outer walls strongly suggest high outer wall selectivity of this intercalation oxidation chemistry.

Using an experimental Kataula plot which correlates electronic transitions and the RBM modes,[31−33] we could assign the majority of the inner tubes within the Raman resonance window of the laser excitation line used (632.8 nm) to metallic types. Similar trends were observed with 514.5 and 488.0 nm (see Supporting Information). Since the Kataula plot was constructed from Raman data on SWNTs with a wide range of diameters (0.7−2.3 nm)[31−33] and the three laser excitation lines together sampled a large population of different nanotube structures, the outer wall selectivity is likely a general phenomena of DWNTs reacted under the intercalation oxidation conditions investigated. Metallic selectivity has important implications for the use of *oso*-DWNTs for electronic applications and will be discussed further at the end of the section.

The disappearance of the outer wall RBMs correlates with the simultaneous decrease of the G band (∼1585 cm^{-1}) and the rise of the D band (∼1280 cm^{-1}), which occurs due to the increased outer wall functionalization. The integrated ratio of the disorder and the graphene vibrational modes (D/G ratio) directly indicates the degree of DWNT functionalization. Additionally, the higher the ratio of the inner-tube RBM intensity to the G band, the higher the outer wall selectivity. To confirm the outer wall selectivity, high resolution TEM was performed on the 10 mL 2 h sample, which had the highest outer wall selectivity according to the RBM/G band ratio, and the 5 mL 24 h sample, which had the highest D/G ratio among the eight reaction conditions investigated. Consistent with the higher Raman D/G ratio, TEM images of the 5 mL 24 h sample revealed etched holes on the nanotube sidewalls and shortened nanotubes with some amorphous carbon coating as a result of overoxidation (Figure 3A and 3B). The results from the 10 mL 2 h sample demonstrated intact inner tubes with an absence of the roughness associated with the oxidized outer walls (Figure 3C and 3D). This outer wall surface morphology is a result of sp^2 hybridized carbons converting to pyramidalized sp^3 by oxidation. The structural contrast between inner tubes and outer walls further supports the conclusion drawn from the Raman data that oxidative functionalization occurred primarily on the outer wall. Length distributions of the samples were quantified using a combination of SEM and the imaging software, ImageJ. Raw, nonoxidized DWNTs featured an average length of 502 ± 341 nm, while the 10 mL 2 h and 5 mL 24 h samples were 361 ± 277 nm and 305 ± 250 nm, respectively. The length distributions for all three samples followed log-normal distribution functions (see Supporting Information). Therefore, the 5 mL 24 h sample had undergone greater oxidative shortening than the 10 mL 2 h sample, which is consistent with the TEM images.

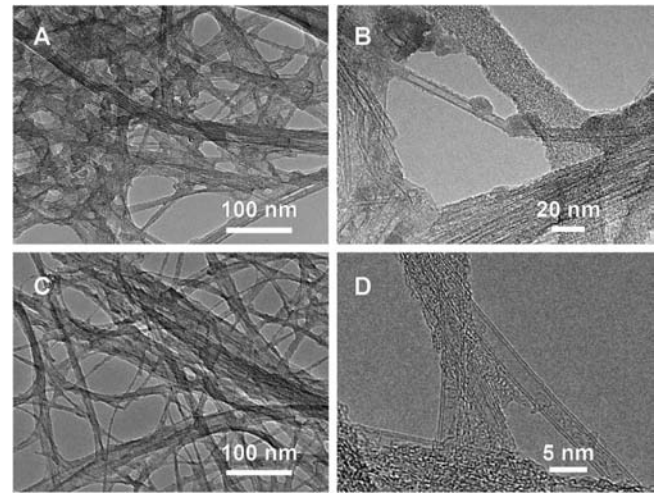

Figure 3. Comparative TEM studies of *oso*-DWNT samples of highest water solubility (A,B: 5 mL 24 h) and higher outer wall selectivity (C,D: 10 mL 2 h) showing two contrasting oxidation products: (A,B) shortened nanotubes with amorphous carbon coating; (C,D) long, exfoliated nanotube bundles with clean wall structures.

The outer wall selectivity can be attributed to the physical protection of the inner tube by the outer wall[34,35] and deliberately controlled reaction conditions. The high aspect ratio of the one-dimensional structure (>1000) can significantly slow the diffusion of the reagents into the inner tubes and thus retard the endohedral reaction pathway.[36] Although there are few studies on DWNT chemistry, it is reasonable to suspect that sulfuric and nitric acids can diffuse into the inner tubes due to their smaller sizes than the opening of the nanotubes. However, the intercalation by oleum opens diffusion pathways for HNO_3 to access the outer wall surface more easily. This mechanism enabled a more homogeneous reaction compared with fluorination[35] or nitric acid alone. The chemistry is straightforward and highly scalable, as it eliminates an initial step involving dispersion by surfactants or organic solvent[13] and allows for homogeneous reactions at high nanotube concentrations.

The chemical nature of the functional groups is −COOH, as shown by high resolution XPS data. The C 1s spectrum for the raw DWNTs shows a dominating peak due to sp^2 hybridized carbon (∼284.5 eV). After oxidation, the content of sp^3 carbon increased and two new peaks at ∼289.0 and ∼285.0 eV appeared, which can be attributed to −COOH (∼6.5% of total carbon signal). Consistent with this assignment, examination of the O 1s region revealed a large increase in oxygen concentration for the oxidized DWNTs as compared to the starting material. The peaks of C−O (∼533.5 eV) and C═O (∼531.9 eV) have a 1:1 area ratio that matches the stoichiometry of the carboxylic acid group (see Supporting Information). The appearance of these surface functional groups after oxidation explains the increased solubility of the DWNTs.

The samples' solubility was further investigated as a function of reactant concentration and reaction time by following the product with UV−vis absorbance and Raman spectroscopy. Because the oxidized nanotubes were soluble in water, a simple

(31) Maultzsch, J.; Telg, H.; Reich, S.; Thomsen, C. *Phys. Rev. B* **2005**, *72*, 205438/1–205438/16.
(32) Telg, H.; Maultzsch, J.; Reich, S.; Thomsen, C. *Phys. Rev. B* **2006**, *74*, 115415/1–115415/5.
(33) Araujo, P. T.; Doorn, S. K.; Kilina, S.; Tretiak, S.; Einarsson, E.; Maruyama, S.; Chacham, H.; Pimenta, M. A.; Jorio, A. *Phys. Rev. Lett.* **2007**, *98*, 067401/1–067401/4.
(34) Green, A. A.; Hersam, M. C. *Nat. Nanotechnol.* **2009**, *4*, 64–70.
(35) Hayashi, T.; Shimamoto, D.; Kim, Y. A.; Muramatsu, H.; Okino, F.; Touhara, H.; Shimada, T.; Miyauchi, Y.; Maruyama, S.; Terrones, M.; Dresselhaus, M. S.; Endo, M. *ACS Nano* **2008**, *2*, 485–488.
(36) Khlobystov, A. N. *Chemistry of Carbon Nanotubes*; Basiuk, V. A., Basiuk, E. V., Eds.; American Scientific Publishers: Stevenson Ranch, CA, 2008; Vol. 3, pp 87−111.

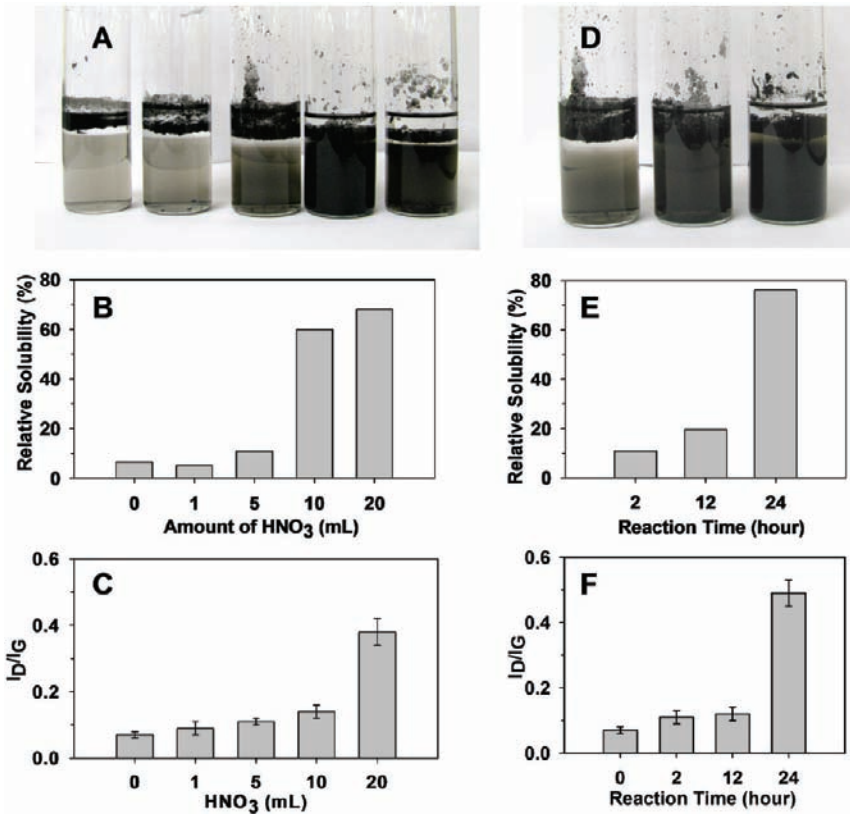

Figure 4. Relative water solubility and degree of functionalization of oxidized DWNTs under increasing amount of HNO_3 at a fixed reaction time of 2 h (A−C) and increasing reaction time using 5 mL of HNO_3 (D−F). (A, D) Solvation competition of oxidized DWNTs in water and hexane. The partitioned samples are shown in order as they appear in the solubility graphs below each image. (B, E) Relative solubility: percent of functionalized DWNTs dissolved in water. (C,F) Degree of functionalization based on Raman I_D/I_G of DWNT samples.

solvation competition between water and an organic solvent, such as hexane, enabled separation of water-soluble nanotubes from the more hydrophobic components. Figure 4A and 4D show photographs of the partitioned DWNT samples (3.0 mg each) in 18 mL of basic water and 7 mL of hexane after being oxidized at different reaction conditions. The darkness of the aqueous layer correlates with an increase in the percentage of nanotubes dissolved. The percentage of water-soluble nanotubes, or relative solubility, at each experimental condition was further quantified by measuring the absorbance of the aqueous layer against an absorbance−concentration working curve. The solubility trends observed were expected. When the reaction time was held constant (2 h), the solubility increased with reactant concentration (1, 5, 10, 20 mL) (Figure 4B). When the reactant concentration was held constant (5 mL), the solubility increased with reaction time (2, 12, 24 h) (Figure 4E). Consistent with the solubility trends, the Raman D/G ratio increases with an increasing amount of nitric acid in addition to increasing reaction time (Figure 4C and 4F). These trends were observed as a result of increased oxidative functionalization of the DWNT samples with increasing either reactant concentration or reaction time.

The maximum relative solubility was achieved by reacting the DWNTs with 5 mL of nitric acid over 24 h. 76% of the DWNTs in this sample dissolved in basic water compared to 68% for the second most soluble sample (20 mL 2 h). The maximum solubility, from the 5 mL 24 h sample, was 760 mg/L. The solubility for the 10 mL 2 h sample, which shows higher outer wall selectivity, was 600 mg/L as calculated from the relative solubility with respect to the 5 mL 24 h sample. High solubility is crucial for potential applications of carbon nanomaterials in a number of areas, especially biomedical applications,[5] composites,[2−4] and solar cells.[6,7] A high density of carboxylic acid groups on the nanotube sidewall will offer a large number of covalent anchoring points. This feature is important for improving solubility and load transfer.[3]

We note that maximum solubility may not correspond with the highest outer wall selectivity. While the maximum solubility was observed with samples reacted with 5 mL of HNO_3 for 24 h, the highest outer wall selectivity was achieved at reaction conditions of 10 mL of HNO_3 for 2 h. This condition mismatch is not surprising since extended reaction time and aggressive reaction conditions tend to produce more functional groups until the nanotube decomposes or each carbon is converted from sp^2 hybridization to sp^3, which results in higher solubility. However, the extreme condition also involves oxidation of the inner tubes. This leads to an overall loss of the desirable electronic and optical properties associated with an sp^2 hybridized network of carbons of a pristine inner tube. Therefore, it is important to

Table 1. Electrical Conductivity of *oso*-DWNTs Thin Films in Comparison with Pristine DWNTs, SWNTs, and Functionalized SWNTs

		Conductivity $S \cdot m^{-1}$ (percentage retained)[a]	
		1.53 μm thick strip	0.15 μm thick strip
Single-walled	Pristine	6.70×10^4	7.24×10^4
	Functionalized	2.65×10^4 (40%)	2.92×10^4 (40%)
Double-walled	Pristine	4.16×10^4	3.81×10^4
	oso-DWNTs	2.75×10^4 (66%)	2.06×10^4 (54%)

[a] Number in parentheses denotes the percentage of electrical conductivity retained after functionalization with respect to the respective pristine nanotubes of similar thickness. All errors are within ±5%.

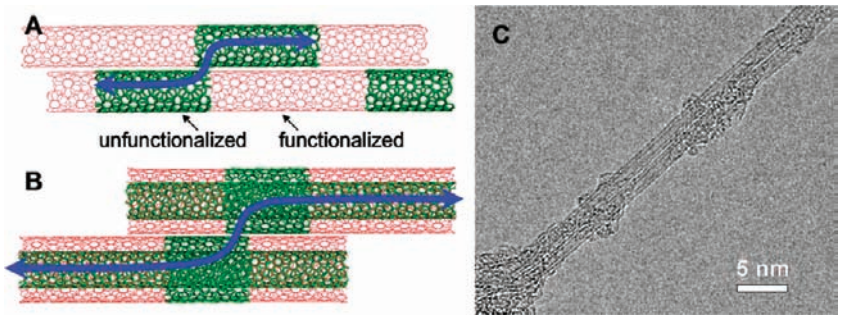

Figure 5. Electrical percolation of *oso*-DWNTs via inner tubes. (A) The broken conductive pathway due to sidewall functionalization of SWNTs. (B) Intact inner tubes extend the electrically conductive pathways. (C) High resolution TEM image showing two *oso*-DWNTs in contact.

balance these competing factors to achieve the highest outer wall selectivity simultaneously with the highest water solubility possible. Although our experiments have yet to exhaust the parameter matrix, the trends we have observed could serve as a useful guide for tuning the reaction conditions for intended applications.

The ability to solubilize metallic nanotubes without causing disruption of their electronic structures opens opportunities to investigate the properties and facilitate applications of metallic nanotubes. Wiring nanostructures with effective electrical contact and percolation is a central challenge in conductive composites, electrical energy storage, and photovoltaics nanoscience.[2−4,7] Remarkably, the electrical conductivity of oxidized DWNTs was much better retained compared to SWNTs. The volume electrical conductivity of an ~1.5 μm thick film prepared from oxidized DWNTs reached 2.75×10^4 S·m^{-1}, or 66% of electrical conductivity was retained after the outer wall selective oxidation. This was 65% higher than what was retained for similarly functionalized HiPco SWNTs (Table 1). The electrical conductivity of the overoxidized DWNTs (5 mL 24 h samples) dropped 47 ± 2% in comparison to the *oso*-DWNTs (10 mL 2 h samples) for both the 1.53 and 0.15 μm films, manifesting the importance of outer wall selectivity. In contrast to functionalized SWNTs, the intact inner tubes of *oso*-DWNTs provide a continuous conductive pathway which is otherwise shortened due to sidewall functionalization (Figure 5).

However, if the outer wall was functionalized, how could the inner tubes make electrical contact with the outer wall and also interconnect with one another so effectively? This puzzle was resolved with high resolution TEM revealing a clustered distribution of functional groups on a carbon nanotube surface (Figure 5C). There are segments of intact outer walls on the order of tens of nanometers which would allow two functionalized DWNTs to contact electrically with the inner tubes. The clustered distribution of functional groups also explains the surprisingly low Raman D/G ratio associated with these oxidized DWNT samples. Typically, the D/G ratio indicates the degree of DWNT functionalization. The D/G ratio increases with an increasing amount of nitric acid in addition to increasing reaction time; however the increase was small. For the 2 h samples, the D/G ratio changed little with respect to that of as-received DWNT material (~0.07 ± 0.01) (Figure 2). Given the high water solubility, the D/G ratio of *oso*-DWNTs was unexpectedly low compared with those of oxidized graphenes[37] and SWNTs functionalized with covalent organic chemistry (~1.0).[38] However, similarly low D/G ratios have been reported for short SWNTs with unfunctionalized side walls.[39] These observations can be well explained by invoking an earlier theoretical prediction by Morokuma et al. that the introduction of sp^3-type defects to a nanotube side wall causes a significant decrease of Raman intensity of the G-band due to the broken symmetry.[40] In contrast to conventional organic covalent chemistry, the preservation of the cylindrical symmetry, as indicated by the observed structural pattern of the oxidized DWNTs, might have retained the Raman intensity of the G-band, hence, showing the relatively low D/G ratio.

These data strongly suggest that the intercalation oxidation occurs preferentially by reaction propagation from existing defects. Such a reaction mechanism and the resulting *oso*-DWNT structures may allow opportunities to tune the interactions of "sticky" nanotubes over a wide range, which was impossible before, to realize extremely low percolation thresholds in nanocomposites.[4] It is also important to note that the starting DWNT samples have a DWNT purity of only 60% as specified by the manufacturer. Of the 60%, the possibility of an inner tube to be metallic is approximately 1/3.[1] Significant improvements are anticipated with enriched DWNTs[34] or if pure metallic types can be separated or synthesized. Ongoing experiments are directed toward addressing these questions. However, the reported *oso*-DWNTs and the more efficient electrical percolation through inner tubes suggest a powerful mechanism to simultaneously improve the dispersion and percolation of carbon nanostructures in conductive composites.

Conclusions

Outer wall selective oxidization of DWNTs was demonstrated by reacting DWNTs with a combination of oleum and nitric acid. The intercalation of oleum between bundled DWNTs presumably opens the diffusion pathways for nitric acid to access the outer walls, resulting in a homogeneous reaction. The outer wall selectivity was confirmed with Raman spectroscopy and high resolution TEM. Outer wall selectivity enables *oso*-DWNT films to retain electrical conductivity in comparison to covalently functionalized SWNTs. The conductivity of an *oso*-DWNTs thin film approached 2.7×10^4 S·m^{-1}, up to 65% better than similarly functionalized SWNTs thin films. The high electrical conductivity was due to electrical percolation of the intact inner tubes via contacts with portions of nonoxidized outer walls.

(37) Park, S.; Ruoff, R. S. *Nat. Nanotechnol.* **2009**, *4*, 217–224.
(38) Chattopadhyay, J.; de Cortez, F.; Chakraborty, S.; Slater, N. K. H.; Billups, W. E. *Chem. Mater.* **2006**, *18*, 5864–5868.
(39) Ziegler, K. J.; Gu, Z.; Peng, H.; Flor, E. L.; Hauge, R. H.; Smalley, R. E. *J. Am. Chem. Soc.* **2005**, *127*, 1541–1547.
(40) Irle, S.; Mews, A.; Morokuma, K. *J. Phys. Chem. A* **2002**, *106*, 11973–11980.

Acknowledgment. We thank Dr. Li-Chung Lai and Dr. Wen-An Chiou for assistance with TEM, Yin Zhang for assistance with SEM, and Prof. Gary Rubloff for access to the Raman microscope. This work was supported by startup funds and a General Research Board Research Support Award from the University of Maryland, a Nano-Biotechnology Initiative Start-up Award from the Maryland Department of Business and Economic Development, and partially supported as part of the Science of Precision Multifunctional Nanostructures for Electrical Energy Storage, an Energy Frontier Research Center funded by the U.S. Department of Energy, Office of Science, Office of Basic Energy Sciences under Award Number DESC0001160. The support of the Maryland NanoCenter and shared experimental facilities support from the NSF MRSEC under Grant DMR 05-20471 are also gratefully acknowledged.

Supporting Information Available: XPS data, length distribution, additional Raman spectra, and complete list of authors for ref 22. This material is available free of charge via the Internet at http://pubs.acs.org

JA910626U